Empirical Formulae for the Influence of Real Film Thickness Distribution on the Capacitance of an EHL Point Contact and Application to Rolling Bearings

Volker Schneider[a], Hai-Chao Liu[a], Norbert Bader[a], Alexander Furtmann[b] and Gerhard Poll[a]

[a]*Institute of Machine Design and Tribology, Leibniz University Hannover, 30823 Garbsen*
[b]*Flender GmbH, 46395 Bocholt, Germany*

ARTICLE INFO

Keywords:
Rolling Bearing
Capacitance
EHL
Bearing Current

ABSTRACT

Electrical bearing capacitance plays an important role in the prediction of harmful bearing currents, which could lead to premature failure of the bearing and the entire drive system. The effect of rolling speed, force, and material parameters on the electrical capacitance of an elliptical contact in elasto-hydrodynamic lubrication has been studied numerically. An empirical equation that describes the relationship between the areas of central film thickness and minimum film thickness of the HERTZ'ian contact area has been derived. Additional, another formula to calculate the total capacitance of a rolling bearing, based only on the HERTZ'ian contact capacitance with the central film thickness as single parameter, has been developed. Finally, a comparison was made between the calculated capacities and measured values.

1. Introduction

The number of drive systems with voltage source inverters is increasing because of advantages in a faster dynamic response and improved efficiency [1]. However, inverter-induced current as a result of steep voltage rise (e.g. capacitive bearing currents, electric discharge machining (EDM) currents and ground currents) may damage the lubricant and surface of rolling element bearings (e.g. grey frosting) and can lead to premature failure of the whole drive system [2]. The harmful EDM current is caused by discharges of electrically loaded elasto-hydrodynamic film (EHL) between raceway and rolling element when a threshold voltage based on a capacitance voltage divider or the bearing voltage ratio (BVR) [3] is surpassed. To predict bearing voltage and EDM current, knowledge about the capacitances of both a single EHL contact and a whole bearing is required.

The capacitance of a model EHL contact can be determined assuming the EHL contact as a plate capacitor

$$C = \epsilon \cdot \frac{A}{d} \tag{1}$$

where $\epsilon = \epsilon_0 \cdot \epsilon_r$ is the absolute permittivity of lubricants, A the contact area, and d is the film thickness of the HERTZ'ian contact zone. In addition, the influence of the regions outside the HERTZ'ian contact zone on the capacitance C_{outside} must be taken into account (see Figure 1).

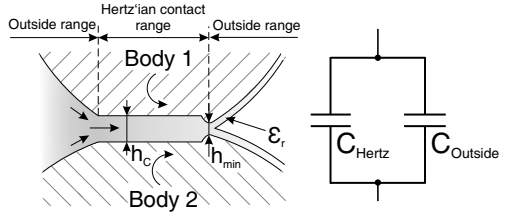

Figure 1: *Electrical analogy model of an EHL contact.*

The total capacitance of a contact $C_{\text{tot,con}}$ is then a sum of both proportions

$$C_{\text{tot,con}} = C_{\text{Hertz}} + C_{\text{outside}} \tag{2}$$

C_{Hertz} may be approximated by

$$C_{\text{hertz,h}_c} = \epsilon_0 \cdot \epsilon_r \cdot \frac{A_{\text{Hertz}}}{h_c} \tag{3}$$

assuming the film thickness inside the HERTZ'ian contact zone being equal to the central film thickness h_c, which can be calculated from empirical equations, e.g. HAMROCK-DOWSON equation for point contacts [4]. Note that the portion of total capacitance contributed from the gap outside the HERTZ'ian contact zone C_{outside} is usually larger than C_{Hertz} [5, 6, 7]. C_{outside} varies with contact geometry and h_c, and it is usually taken into account in the total capacitance determination of a contact $C_{\text{tot,con}}$ through a factor k_c

$$k_c = \frac{C_{\text{tot,con}}}{C_{\text{Hertz,h}_c}} \tag{4}$$

which indicates the ratio between total capacitance and the capacitance of the HERTZ'ian contact for a given contact. An ideal k_c factor would then take into account the effect of the deformations of the bodies outside the HERTZ'ian contact zones, as well as the influence of the real film thickness distribution inside the HERTZ'ian contact on the total capacitance. When looking at the contact area an EHL film is characterized by a flat zone with a nearly constant film thickness h_c along the central line of entrainment direction. Close to the outlet, a constriction with thinner film thickness has been proven both experimentally and theoretically [8]. Typically, the EHL film of point contacts has a horse-shoe shaped constriction. Through Eq. 1, it is easy to understand that a thinner film leads to increased capacitance. Therefore, one aim of this work is to investigate the influence of

Nomenclature

Greek Symbols

α_p	pressure-viscosity coefficient	Pa^{-1}
α_s	BODE-parameter	–
α_t	temperature-viscosity coefficient	K^{-1}
$\beta(\vartheta)_T$	isothermal compressibility	1/bar
β_K	temperature coefficient $\approx 0.00651/K$	1/K
δ_r	contact deformation or deflection	m
ϵ	absolute permittivity	F/m
ϵ_0	electric constant $= 8.8541878 \times 10^{-12}$	A s/V m
ϵ_r	relative permittivity	–
ϵ_{air}	relative permittivity of air ≈ 1.0006	–
η_0	dynamic viscosity for Murch/Wilson	Pa s
η_0	dynamic viscosity for speed parameter U	mPa s
λ	thermal conductivity of lubricant	W/mK
$\mathcal{E}$	complete elliptical integral of second order	–
ν	POISSON'S ratio	–
ν_{rs}	kinematic operating viscosity of lubricant	mm^2/s
Φ_{rs}	replenishment/starvation reduction factor	–
Ψ	azimuth angle	°
ρ	curvature	1/m
φ	angle	°
ϱ	density	kg/m^3
ϱ_0	density at 15 °C	kg/m^3
ϱ_s	BODE-parameter	–
ϑ	temperature	°C

Roman Symbols

$\bar{v}$	entrainment velocity	m/s
A	area	m^2
a	greater half-widths of contact ellipse	m
$A_1 ... A_4$	BODE-parameters	–
$a_1 ... a_5$	BODE-parameters	–
a_V	thermal expansivity	1/K
b	lesser half-widths of contact ellipse	m
C	capacitance	F
C_{MW}	thermal correction factor	–
D	bearing outside diameter	mm
d	bearing bore diameter	mm
d_{gap}	thickness of gap between capacitor plates	m
E	elastic modulus	Pa
E'	equivalent elastic modulus	Pa
F	force	N
G	dimensionless material parameter	–
H	dimensionless film thickness	–
h	film thickness	m
K_0	isothermal bulk modulus at zero pressure	GPa
K_0'	change rate of isothermal bulk modulus	–
$k_1 ... k_3$	BODE-parameters	–
k_c	ratio between C_{total} and C_{Hertz,h_c}	–
k_e	ellipticity parameter $k = \frac{a}{b}$	–
K_Z	Bearing type related geometric constant $= 3.1$ single row deep groove ball bearing $= 5.1$ cylindrical roller bearing with cage	–
K_{rs}	replenishment/starvation constant $= 3 \cdot 10^{-8}$ low level oil bath/oil jet lubrication $= 6 \cdot 10^{-8}$ grease/oil-air lubrication	–
k_{vh}	ratio between $C_{Hertz,h_{real}}$ and C_{Hertz,h_c}	–
L	thermal load parameter	–
m_r	dimensionless roughness value	–
n	rotational speed	1/min
p	pressure	Pa
P_d	radial clearance	m
Q	contact load	N
R	composite radius	m
r	radius	m
R_Z	maximum height of roughness profile	m
$t_r(\beta)$	directional value	–
U	dimensionless speed parameter	–
U_b	bearing voltage	V
U_{CM}	common mode voltage	V
V	volume at T and p	m^3
V_0	volume at $p = 0$	m^3
W	dimensionless load parameter	–
w	total deflection of two solid bodies $w = 2 \cdot w_0$	m
w_0	deflection of one solid body	m
Z	number of rolling elements	–

Subscripts

$brng$	bearing
c	central
con	contact
r	roughness
RE	rolling element
rs	replenishment/starvation
th	thermal
tot	total
x	x-direction
y	y-direction

the thinner film thickness area on the total capacitance of a contact. In literature the real EHL film shape was usually ignored by assuming a uniform thickness of h_c in simulations [5, 6, 7, 9, 10, 11, 12].

To consider the contribution of the capacitance outside the HERTZ'ian zone, BARZ [13] and WITTEK ET AL. [10] used a universal value of $k_c = 3.5$ giving a good approximation for axially loaded rolling bearings. However, $C_{outside}$ is a func-

tion of film thickness and JABLONKA ET AL. [7] showed that k_c increases almost linearly from 1 to 3 as a function of film thickness from 15 nm to 250 nm for a model EHL contact. For a radially-loaded bearing, the rolling elements have different k_c values due to varying loading distributions and carrying areas. In literature, there is no appropriate formula to describe k_c as a function of film thickness or the related DOWSON-HIGGINSON dimensionless groups, i.e. U, G, W.

Note that, using Eq. 1 and Eq. 2 also represent a possibility for mean film thickness measurement of an EHL contact as long as the total capacitance can be measured experimentally. This has been applied e.g. by [9, 14, 15, 16, 17, 7, 18]. Another potential approach to determine $C_{\mathrm{tot,con}}$ is to calculate the deformation of the outside region using approximation formulae e.g. [19] in order to derive C_{outside} and then add this to C_{Hertz}. This approach would take into account the influence of the deformation of the outer region, but would neglect the influence of the area of the film thickness lower than h_c. If the regions of lower film thickness play a role for C_{Hertz}, a formula to describe the extent as a function of film thickness or the DOWSON-HIGGINSON parameters would be convenient for engineering applications to allow for a more accurate prediction of the total contact capacitance.

This study presents two empirical formulae accounting for the influence of real film distribution on the capacitance of an elliptical EHL contact based on numerical EHL simulations using multigrid techniques.

Analytical Method using k_c-Factor
The factor $k_c(U, G, W, k_e)$ expresses the ratio between the HERTZ'ian zone capacitance and the total contact capacitance as described in e.g. [6, 20, 21]. In the area of the HERTZ'ian contact, the presented factor is based on the pressure-dependent permittivity distribution compared to the preliminary work. The k_c-factor thus includes the influences of the region of lower film thickness and the region outside the EHL-contact zone on the total contact capacitance. It is therefore possible to infer the total capacitance of the contact from the determinable capacitance of the HERTZ'ian contact with the aid of the k_c-factor.

Analytical Method using k_{vh}-Factor
The $k_{vh}(U, G, W, k_e)$-factor describes the relationship between the capacitance of the HERTZ'ian contact area at constant lubricant film height h_c and the capacitance considering the real lubricant film distribution of an EHL contact. The factor is therefore used for a more precise description of the HERTZ'ian capacitance. The influence of the outside region on the total contact capacitance has to be determined additionally, for example, by an analytical determination of the deformations outside the contact zone.

In order to determine the factor k_c and k_{vh}, EHL contact capacitances for different speeds, materials and loads have been determined analytically and in a numerical simulation. By comparing the results from these two approaches, the factors were determined. The analytical and numerical approach is explained in detail in the following. The proposed two formulae have been applied to analytical capacitance calculations for a rolling element bearing under axial, radial and combined load conditions. Capacitance measurements of a rolling bearing have been carried out for comparison and validation of the proposed factors.

2. Analytical Capacitance Calculation

2.1. Calculation for a Single EHL Contact

There are two different approaches to calculate the total capacitance for a single EHL contact. The basic procedures are explained below.

Analytical Method using k_c-Factor
For this approach it is only necessary to calculate the capacitance of the HERTZ'ian contact and multiply it by the factor k_c (see Eq. (53)).

$$C_{\mathrm{tot,con}} = \epsilon_0 \cdot \epsilon_r(p, \vartheta) \cdot k_c \cdot \frac{A_{\mathrm{Hertz}}(F_N, R, E')}{h_c(\bar{v}, F_N, R, E', \eta(p, \vartheta))} \quad (5)$$

Analytical Method using k_{vh}-Factor
For the second method it is necessary to determine the deformed regions outside the HERTZ'ian contact zone analytically. This approach is useful when the influence of the minimum film thickness on the HERTZ'ian capacitance is unknown. Therefore the different portions that are included in the calculation of $C_{\mathrm{tot,con}}$ must be clarified firstly.

Figure 2 shows the different regions that are included in the capacitance calculation. The capacitance to be calculated is basically divided into three regions, the outside regions and the EHL contact region itself. For the outside regions, a distinction is made between the capacitance of the inlet and outlet region $C_{\mathrm{inl.}}$ and $C_{\mathrm{outl.}}$. In a simplified manner, the outlet region $C_{\mathrm{outl.}}$ is assumed to span a right angle characterized by a mixture of air and lubricant. The fundamental difference in the calculation of the capacitances for both regions is the lubricant permittivity, which can be understood in the outlet region as a series connection of different permittivities of air and a thin layer of oil assumed to be of the thickness $0.5 \cdot h_c$ at the top and bottom solid surfaces, because it is the assumed amount of lubricant that can get through the narrow EHL-contact.

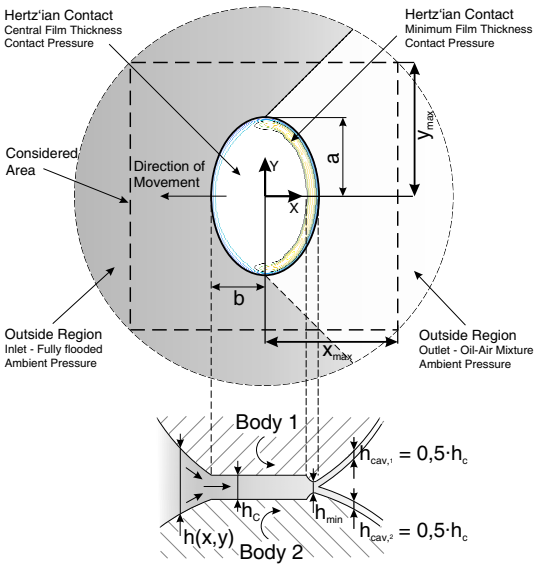

Figure 2: *Different regions present in an EHL contact of two lubricated bodies.*

The inlet region, is assumed to be fully flooded. Thus in Cartesian coordinates:

$$C_{\text{inl.}} = \iint_{\text{A}} \epsilon_0 \cdot \epsilon_{\text{r}}(p_0, \vartheta) \cdot \frac{A_{\text{incr}}}{h(x,y)}\, dx\, dy \tag{6}$$

For $x > 0$:

$$x \;<\; |y| - a \;\;\wedge\;\; \frac{x^2}{b^2} + \frac{y^2}{a^2} > 1$$

and for $x < 0$

$$-y_{\max} < y < y_{\max} \;\;\wedge\;\; \frac{x^2}{b^2} + \frac{y^2}{a^2} > 1$$

Where:

$$x_{\max} = y_{\max} = \frac{\sqrt{2}}{2} \cdot r_{\text{RE}}$$

The capacitance of the outlet region can be described as follows:

$$C_{\text{outl.}} = \iint_{\text{A}} \left(\underbrace{\frac{h(x,y) - h_{\text{c}}}{\epsilon_0 \cdot \epsilon_{\text{air}} \cdot A_{\text{incr}}}}_{\text{Air}} + \underbrace{\frac{h_{\text{c}}}{\epsilon_0 \cdot \epsilon_{\text{r}} \cdot A_{\text{incr}}}}_{\text{Lubricant}} \right)^{-1} dx\, dy \tag{7}$$

$$A = \left[-x_{\max}, x_{\max}\right] \times \left[-y_{\max}, y_{\max}\right]$$

When:

$$x \;>\; |y| - a \;\;\wedge\;\; x > 0 \;\;\wedge\;\; \frac{x^2}{b^2} + \frac{y^2}{a^2} > 1$$

To describe the relationship between the HERTZ'ian capacitance by assuming a constant central film thickness and the HERTZ'ian capacitance based on the real film thickness distribution, a factor k_{vh} is introduced which depends on the dimensionless parameters U, G, W and k_{e}.

$$k_{\text{vh}}(U, G, W, k_{\text{e}}) = \frac{C_{\text{Hertz,real}}}{C_{\text{Hertz,h}_{\text{c}}}} \tag{8}$$

Eq. (1) is therefore modified so that the capacitance of the contact region considering a realistic film thickness distribution is:

$$C_{\text{Hertz,real}} = \epsilon_0 \cdot \epsilon_{\text{r}}(p, \vartheta) \cdot k_{\text{vh}}(U, G, W, k_{\text{e}}) \cdot \frac{A_{\text{Hertz}}(F_{\text{N}}, R, E')}{h_{\text{c}}(\bar{v}, F_{\text{N}}, R, E', \eta(p, \vartheta))} \tag{9}$$

The total capacitance of a contact is then the sum of the individual parts:

$$C_{\text{tot,con}} = C_{\text{inl.}} + C_{\text{outl.}} + C_{\text{Hertz,real}} \tag{10}$$

2.2. Calculation for a Rolling Bearing

If the bearing is purely axially-loaded, all rolling elements may be regarded as being equally loaded. If the capacitance model for a single contact is transferred to a radially loaded rolling bearing, it must be considered that not every rolling element is loaded equally. Under radial load, a load zone is formed in which it is possible to calculate the film thickness with EHL formulas such as the formulae provided by HAMROCK and DOWSON [4] (see Sec. 3.1). For rolling elements outside the load zone, the distances between a rolling element and a raceway can be calculated according to the approach described in [22]. Taking into account the bearing clearance P_{d} and the ring radial shift δ_{r} at $\Psi = 0$, the radial deflection, respectively clearance, at every angle δ_Ψ can be calculated using the formula:

$$\delta_\Psi = \delta_{\text{r}} \cdot cos\Psi - 0.5 \cdot P_{\text{d}} \tag{11}$$

It is assumed that the rolling element outside the load zone is placed centrally between inner and outer ring. Since no contact zone is established, the calculation is based on non deformed rolling elements and raceways and is integrated over the considered area as follows:

$$C_{\text{tot,con,unloaded}} = \iint_{\text{A}} \epsilon_0 \cdot \epsilon_{\text{r}}(p_0, \vartheta) \cdot \frac{A_{\text{incr}}}{h(x,y)}\, dx\, dy \tag{12}$$

$$A = \left[-x_{\max}, x_{\max}\right] \times \left[-y_{\max}, y_{\max}\right]$$

In order to determine the total capacitance of a bearing, it is additionally necessary to consider the type of cage material i.e. electrically conductive (steel or brass cage) or insulating (polyamide cage). Figure 3 shows the electrical equivalent circuit diagram of a ball bearing under full film lubrication, in which each contact can be represented as a parallel connection of capacitor and resistor [23]. The resistor is of interest for modelling the electrical arc discharge across the contact. By reaching the critical breakdown voltage of the lubricant, the resistor value can be assumed to change over

time. This work focuses on modelling the capacitance in order to estimate the electrical load on the rolling bearing. The modelling of the resistor has already been described in detail in [24]. With a conductive cage, the rolling elements are short-circuited among each other (assuming that there is contact between rolling element and cage). In addition, every inner ring (IR) contact and every outer ring (OR) contact is short-circuited. This results in a parallel connection of the IR and OR contacts which are connected in series. To calculate the total capacitance for a bearing with conductive cage and Z rolling elements, Eq. (13) is obtained [6].

$$C_{\mathrm{tot,brng}} = \frac{\sum_{\mathrm{i}=1}^{Z} C_{\mathrm{tot,con,IR,i}} \cdot \sum_{\mathrm{i}=1}^{Z} C_{\mathrm{tot,con,OR,i}}}{\sum_{\mathrm{i}=1}^{Z} C_{\mathrm{tot,con,IR,i}} + \sum_{\mathrm{i}=1}^{Z} C_{\mathrm{tot,con,OR,i}}} \tag{13}$$

For rolling bearings with an insulating cage, the IR and OR contact are in a series connection. Each rolling element is then connected in parallel with the others. This results in Eq. (14).

$$C_{\mathrm{tot,brng}} = \sum_{\mathrm{i}=1}^{Z} \frac{C_{\mathrm{tot,con,IR,i}} \cdot C_{\mathrm{tot,con,OR,i}}}{C_{\mathrm{tot,con,IR,i}} + C_{\mathrm{tot,con,OR,i}}} \tag{14}$$

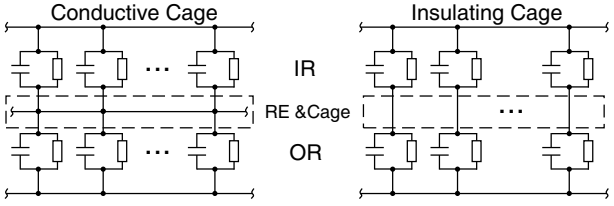

Figure 3: *Electrical equivalent circuit of a bearing with different cage materials [6].*

3. Distance Calculation for Capacitance Determination

The calculated capacitances for both approaches strongly depend on the film thickness in EHL contacts and the resulting distances outside EHL contact due to the deflection of the bodies. In the following two sections, additional modifications that are included in the film thickness calculation will be introduced.

3.1. Film Thickness and Contact Size Formulae for EHL Contacts

The formula to calculate the dimensionless central film thickness of point contacts H_{c} presented by Hamrock and Dowson [4] was chosen to be the basis of the calculation.

$$H_{\mathrm{c}} = \frac{h_{\mathrm{c}}}{R_{\mathrm{x}}} = 2.69 \cdot G^{0.530} \cdot U^{0.67} \cdot W^{-0.067} \cdot (1 - 0.61 \cdot e^{-0.73 \cdot k_{\mathrm{e}}}) \tag{15}$$

This equation is based on the dimensionless parameters for material G, load W and speed U. They are expressed as:

$$U = \frac{\eta_0 \bar{v}}{E' R_{\mathrm{x}}} \tag{16}$$

$$G = \alpha_{\mathrm{p}} E' \tag{17}$$

$$W = \frac{Q}{E' R_{\mathrm{x}}^2} \tag{18}$$

With the elasticity modul E and and the Poisson ratio ν of contacting bodies $1, 2$ the equivalent elastic modulus E' is then defined as

$$E' = 2 \left(\frac{1 - \nu_1^2}{E_1} + \frac{1 - \nu_2^2}{E_2} \right)^{-1} \tag{19}$$

With convex curvatures defined as negative, the composite radius R is

$$R = \left(\frac{1}{R_{\mathrm{x}}} + \frac{1}{R_{\mathrm{y}}} \right)^{-1} = \left(\frac{1}{r_{1_{\mathrm{x}}}} + \frac{1}{r_{2_{\mathrm{x}}}} + \frac{1}{r_{1_{\mathrm{y}}}} + \frac{1}{r_{2_{\mathrm{y}}}} \right)^{-1} \tag{20}$$

The area of the contact ellipse can be determined by semi-axes a and b of the contact ellipse. These can be determined in a good approximation using the formulae from Hamrock and Dowson [4].

$$a = \sqrt[3]{\frac{6 k_{\mathrm{e}}^2 \mathcal{E} Q}{\pi \sum \rho E'}} \tag{21}$$

$$b = \sqrt[3]{\frac{6 \mathcal{E} Q}{\pi k_{\mathrm{e}} \sum \rho E'}} \tag{22}$$

Using the composite radius taken from Eq. (20), the curvature of the bodies $\sum \rho$ and the provided fits for the ellipticity parameter k and the complete elliptical integral of second order $\mathcal{E}$ (which are marked as $\bar{k}_{\mathrm{e}}$ and $\bar{\mathcal{E}}$), the semi-axes can be calculated.

$$\sum \rho = \frac{1}{R} \tag{23}$$

$$\bar{k}_{\mathrm{e}} = 1.0339 \cdot \left(\frac{R_{\mathrm{y}}}{R_{\mathrm{x}}} \right)^{0.636} \tag{24}$$

$$\bar{\mathcal{E}} = 1.0003 + \frac{0.5968}{R_{\mathrm{y}} / R_{\mathrm{x}}} \tag{25}$$

With the above formulae it is now possible to calculate the central distance between the contracting bodies as well as the size of the contact zone. However, the real film thickness distribution of an EHL contact still depends on additional effects that are not represented by Eq. (15). These effects are explained below and the influence of each on the film thickness is highlighted. Ultimately, the capacitance is calculated with the reduced film thickness, which takes the various effects into account.

3.1.1. Thermal Influence on EHL Film Thickness

The influence of the temperature rise due to reverse oil flow in the inlet zone may be considered based on the work of MURCH and WILSON [25], which reduces the film thickness through a thermal correction factor C_{MW}:

$$C_{\mathrm{MW}} = \frac{3.94}{3.94 + L^{0.62}} \tag{26}$$

L describes the thermal load parameter:

$$L = \frac{\eta_0 \cdot \alpha_{\mathrm{t}} \cdot \bar{v}}{\lambda} \tag{27}$$

The reduced film thickness is then calculated according to the following formula:

$$h_{\mathrm{c,th}} = h_{\mathrm{c}} \cdot C_{\mathrm{MW}} \tag{28}$$

3.1.2. Starvation Influence on EHL Film Thickness

Another influence factor on the film thickness is starvation, where the lubricant does not have enough time to replenish the contact. This results in a reduced inlet lubricant supply and a reduced oil film thickness. This may be represented by the *kinematic replenishment/starvation reduction factor* Φ_{rs} given by SKF [26].

$$\Phi_{\mathrm{rs}} = \frac{1}{\mathrm{e}^{[K_{\mathrm{rs}} \nu_{\mathrm{rs}} n(d+D)\sqrt{\frac{K_Z}{2(D-d)}}]}} \tag{29}$$

$$h_{\mathrm{c,th,rs}} = h_{\mathrm{c,th}} \cdot \Phi_{\mathrm{rs}} \tag{30}$$

3.1.3. Roughness Influence on EHL Film Thickness

A higher roughness of both contacting bodies leads to an increased electrical capacitance and therefore has the same effect as a reduced film thickness. This reduction was investigated by KREIL [27] and is summarized in the following formula:

$$\Delta h_{\mathrm{r}} = m_{\mathrm{r}} \cdot R_{\mathrm{Z}} \tag{31}$$

With the maximum height of the profile R_{Z} and the dimensionless roughness value m_{r}:

$$m_{\mathrm{r}} = 0.3 \cdot ln(2 \cdot \bar{v} + 55) + t_{\mathrm{r}}(\beta) \tag{32}$$

The directional value $t_{\mathrm{r}}(\beta)$ considers the orientation of the roughness grooves that correspond to the direction during grinding.

$$t_{\mathrm{r}}(\beta) = \begin{cases} -0.0992 : \beta = 0°(longit.\ grinding) \\ -1.0600 : \beta = 90°(transv.\ grinding) \end{cases} \tag{33}$$

The film thickness then reduces to:

$$h_{\mathrm{c,th,rs,r}} = h_{\mathrm{c,th,rs}} - \Delta h_{\mathrm{r}} \tag{34}$$

3.2. Distance Determination of Deflected Outside Areas

The surfaces outside the HERTZ'ian contact zone also experience a change in geometry due to the elastohydrodynamic pressure. This directly affects the capacitance calculations for the contact. BRUESER [19] derived approximation Formulae ((35),(36), (37), (38), (39)) for the deflection of two arbitrary curved bodies based on the work of TIMOSHENKO [28]. BRUESER made the assumption that the deflected area have the same radius as the undeflected body, but with a shifted center (see Figure 4).

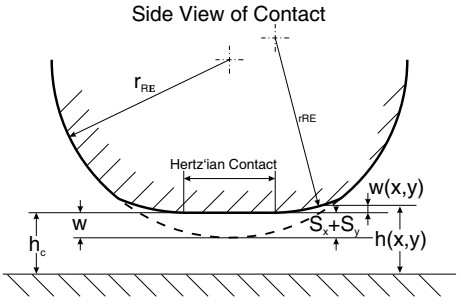

Figure 4: *Distances between a deflected body and a plane - side view [19].*

Assuming that there is a pressure distribution according to HERTZ, the maximum deformation occurs at the center. In polar coordinates we get:

$$w_0 = \frac{8 \cdot (1 - \nu^2)}{\pi \cdot E} \cdot p_0 \cdot \int_0^{\frac{\pi}{2}} \int_0^{r_{\max}} \sqrt{1 - \left(\frac{r_{\mathrm{RE}} \cdot cos\varphi}{b}\right)^2 - \left(\frac{r_{\mathrm{RE}} \cdot sin\varphi}{a}\right)^2}\, dr d\varphi \tag{35}$$

The elliptical contact area is limited by (see Figure 5):

$$r_{\max} = \sqrt{\frac{1}{\left(\frac{r_{\mathrm{RE}} \cdot cos\varphi}{b}\right)^2 + \left(\frac{r_{\mathrm{RE}} \cdot sin\varphi}{a}\right)^2}} \tag{36}$$

With semi-axes a and b calculated with Eq. (21) and (22). The replacement contour of the deflected area then intersects the undeflected area at a distance a_1 and b_1 from the center (see Figure 5). These points of intersection are calculated using quadratic equations Eq. (37) and Eq. (38) given by BRUESER.

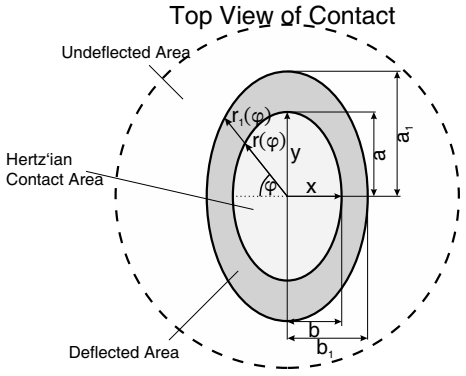

Figure 5: *Different areas of a deflected body - top view [19].*

$$b_1^2(4b^2+w^2)-b_1(bw^2+4b^3)+w^2(\frac{w^2}{16}+\frac{b^2}{2}-r_{\mathrm{RE}}^2)+b^4=0 \tag{37}$$

and

$$a_1^2(4a^2+w^2)-a_1(aw^2+4a^3)+w^2(\frac{w^2}{16}+\frac{a^2}{2}-r_{\mathrm{RE}}^2)+a^4=0 \tag{38}$$

With the calculated points of intersection it is now possible to determine the film thickness between the two surfaces of a contact. In comparison to Figure 4, the formula for the deformed area is obtained.

$$h(x,y)=h_0+S_{\mathrm{x}}+S_{\mathrm{y}}+w(x,y)-w \tag{39}$$

Where:
$S_{\mathrm{x}}=\frac{x^2}{2\cdot R_{\mathrm{x}}}$
$S_{\mathrm{y}}=\frac{y^2}{2\cdot R_{\mathrm{y}}}$

3.3. Electrical Parameters for Capacitance Calculation

The last point to be clarified concerns the physical property of the relative permittivity ϵ_{r}, which varies with temperature and pressure. The density ϱ is directly related to the temperature and pressure. As more molecules are compacted into a certain volume when the lubricant is compressed, the electrical polarization is increased correspondingly [29]. Several ways for the permittivity calculation will be shown and discussed.

3.3.1. Temperature- and Pressure dependent Relative Permittivity

A model to calculate the relative permittivity of a lubricant is the modified Clausius-Mossotti equation [30, 31, 32]. It is based on the temperature and pressure-dependent change in density of the lubricant.

$$\epsilon_{\mathrm{r}}(p,\vartheta)=\frac{\epsilon_{\mathrm{r0}}+2+2\cdot(\epsilon_{\mathrm{r0}}-1)\cdot\varrho(p,\vartheta)/\varrho_0}{\epsilon_{\mathrm{r0}}+2-(\epsilon_{\mathrm{r0}}-1)\cdot\varrho(p,\vartheta)/\varrho_0} \tag{40}$$

The Clausius-Mossotti-equation requires knowledge of the reference density ϱ_0 and and reference relative permittivity ϵ_{r0}. The reference density at 15 °C is usually provided in lubricant data sheet and the reference relative permittivity can be determined experimentally at ambient pressure, see for example Wittek [20].

Table 1
Parameters of 75W-90 gear oil. Extract of Furtmann *[6].*

Parameter	Value
ϱ_{s}	1032.9770508
α_{s}	0.0005829
a_1	0.0997101
a_2	4508.5515539
a_3	−13.1593486
a_4	0.0112271
a_5	−0.0000028
A_1	0.0209645
A_2	4.5773726
A_3	816.7267611
A_4	0.0018826
k_1	0.0039212
k_2	0.0031227
k_3	0.0005351

A different approach is provided in form of the Bode equation [33, 34] which is based on measurements using a quartz viscometer. It also describes the temperature- and pressure dependence of viscosity of the lubricant.

$$\epsilon_{\mathrm{r}}(p,\vartheta)=\epsilon_{\mathrm{r}}(\vartheta)+k_3\cdot[\varrho(p,\vartheta)-\varrho(\vartheta)] \tag{41}$$

With:

$$\epsilon_{\mathrm{r}}(\vartheta)=k_1\cdot\beta(\vartheta)_{\mathrm{T}}^{-0.5}\cdot\varrho(\vartheta)^{1/6}+k_2\cdot\vartheta \tag{42}$$

$$\beta(\vartheta)_{\mathrm{T}}=\frac{a_1}{a_2+a_3\cdot\vartheta+a_4\cdot\vartheta^2+a_5\cdot\vartheta^3} \tag{43}$$

Bode uses the parameters $a_1..a_5$, $A_1..A_4$, ϱ_{s}, α_{s} and $k_1..k_3$ in his equations which need to be determined experimentally using a high pressure viscometer in order to describe the lubricant properties more precisely. Knowledge of the reference density and reference relative permittivity, like in Eq. (40), is also necessary. An exemplary set of parameters is summarized in Table 1 for a 75W-90 gear oil, which was used in this study. The relative permittivity of the used 75W-90 oil is plotted over pressure at different temperatures in Figure 6.

This work will use the Bode-equations for this specific characterized lubricant. As shown by Furtmann [6], they express the lubricant physical properties more precisely and form a solid basis for the capacitance calculation.

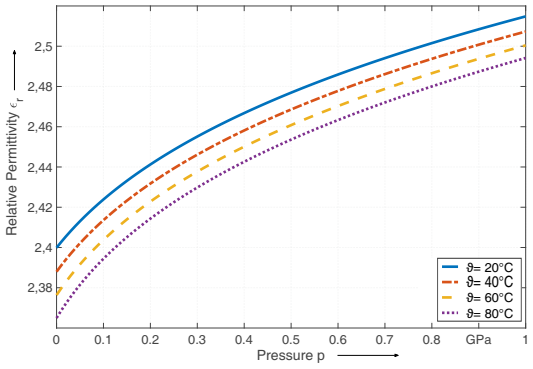

Figure 6: *Pressure and temperature dependent relative permittivity using the equations provided by* BODE.

3.3.2. Temperature- and Pressure dependent Density

The two permittivity equations in the last section require the pressure and temperature dependent density $\varrho(p, \vartheta)$. An often used approach is the density equation provided by DOWSON AND HIGGINSON [35] with temperature influence taken into account.

$$\varrho(p,\vartheta) = \varrho_0 \cdot \left(1 + \frac{0.5988 \times 10^{-9} p}{1 + 1.697 \times 10^{-9} p} - 0.00065(\vartheta - \vartheta_R)\right) \tag{44}$$

Eq. (44) was derived at relatively low pressures (< 350 MPa). A more precise correlation suitable for high pressures would be the TAIT-equation of state [36, 37]. It describes the Volume V of the material at a certain temperature and pressure relative to the volume at ambient pressure V_0.

$$\frac{V}{V_0} = 1 - \frac{1}{1 + K_0'} \ln\left(1 + \frac{p}{K_0(\vartheta)}(1 + K_0')\right) \tag{45}$$

where $K_0(\vartheta)$ is a temperature modified version of K_0

$$K_0(\vartheta) = K_{00} \exp(-\beta_K \vartheta) \tag{46}$$

where K_{00} is K_0 at zero absolute temperature. Additionally the volume at ambient pressure V_0 relative to the volume V_R at the reference temperature ϑ_R is calculated as:

$$\frac{V_0}{V_R} = 1 + a_V(\vartheta - \vartheta_R) \tag{47}$$

A set of parameters for typical lubricants is provided by BAIR and shown in table 2.

BODE offers another group of equations for the description of pressure and temperature dependences of density and viscosity, which, like Eqs. 41 to 43, are based on experimentally determined coefficients.

$$\varrho(p,\vartheta) = \frac{\varrho(\vartheta)}{1 - a_1 \cdot \ln\left(\frac{a_2 + a_3 \cdot \vartheta + a_4 \cdot \vartheta^2 + a_5 \cdot \vartheta^3 + p}{a_2 + a_3 \cdot \vartheta + a_4 \cdot \vartheta^2 + a_5 \cdot \vartheta^3}\right)} \tag{48}$$

with

$$\varrho(\vartheta) = \varrho_s \cdot (1 - \alpha_s \cdot \vartheta) \tag{49}$$

Table 2
General set of parameters for TAIT *EOS by* BAIR *[38].*

Parameter	Value
K_0'	11
K_0	9 GPa
a_V	8×10^{-4} 1/K
β_K	0.0065 1/K

Table 3
Variation range of dimensionless parameters for EHL-simulation.

Parameter	Variation range
U	$0.56...22.52 \cdot 10^{-11}$
G	3300...4615.4
W	$3.44...298.58 \cdot 10^{-6}$
k_e	3.125...7.878

$$\eta(p,\vartheta) = A_1 \cdot \exp\left(\frac{A_2 \cdot \varrho(p,\vartheta)}{\varrho_g(\vartheta) - \varrho(p,\vartheta)}\right) \tag{50}$$

$$\varrho_g(\vartheta) = A_3 \cdot (1 + A_4 \cdot \vartheta) \tag{51}$$

The set of BODE-parameters for the 75W-90 oil used is also given in Table 1.

4. Numerical Simulation for the two formulae k_c and k_{vh}

In order to determine the factors $k_c(U, G, W, k_e)$ and $k_{vh}(U, G, W, k_e)$ based on a realistic film thickness distribution, the multigrid method introduced into EHL by LUBRECHT AND VENNER [39, 40] is used to solve the coupled Reynolds, surface elastic deformation and load balance equations. Results of this multigrid method were already presented in the work of LIU [41], where he pointed out the effect of solid body temperatures on EHL traction, film thickness and film temperature rise.

Simulations were carried out for a broad 'U, G, W, k_e'- parameter range. The speed and therefore the parameter U have been varied for each load selected. In order to include the influence of the geometry into the simulation, the ellipticity factor k_e was selected in a way that the geometries of inner- and outer ring contacts of a 6206 and 6008 deep groove ball bearing (DGBB) were represented. In addition, parameter G was adjusted for each parameter combination of U, W and k_e using the piezoviscous properties of three different oils. An overview of the range of the parameters is given in Table 3.

As is shown in Figure 7 it becomes apparent that the film thickness distribution is by no means constant. This non-uniform film thickness distribution makes it necessary to determine the relation between the analytically determinable central film thickness h_c and the real film shape, that is, the k_{vh} and k_c factor. For rapid engineering application it would

be useful to still rely on the analytical HAMROCK and DOWSON equations combined with the k_{vh} and k_c factor.

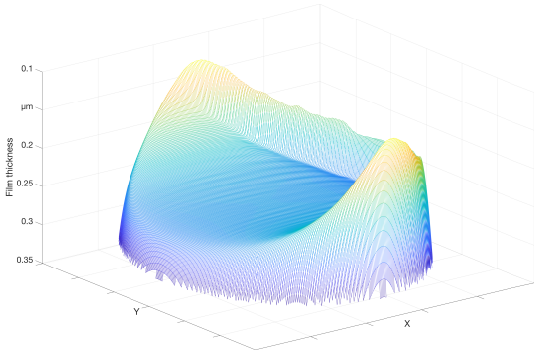

Figure 7: *Film thickness distribution of an EHL-contact result of multigrid-calculation. The area is shown inverted for better illustration* ($U = 0.562 \cdot 10^{-11}, G = 0.46154 \cdot 10^{4}, W = 3.44074 \cdot 10^{-6}, k_e = 3.125$).

4.1. Determination of Factor k_{vh}

Based on the analysis of the obtained numerical results from the multigrid-method, the factor $k_{vh}(U, G, W, k_e)$ is determined. It describes the ratio between the capacitance of the HERTZ'ian contact area using the realistic film thickness distribution obtained through the simulation and the HERTZ'ian contact capacitance determined analytically by assuming a uniform h_c central film thickness distribution.
First, the capacitance is calculated based on the numerically calculated real film thickness (as shown in Figure 7) and pressure distribution (see Figure 8) which clearly shows the typical pressure distribution of an EHL contact with the PETRUSEVICH-pressure-spike [42] in the outlet region.

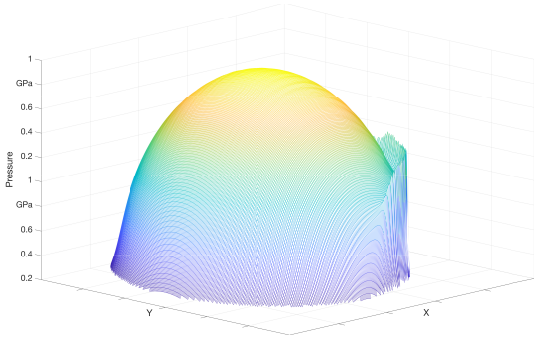

Figure 8: *Pressure distribution of an EHL contact result of multigrid-calculation* ($U = 0.562 \cdot 10^{-11}, G = 0.46154 \cdot 10^{4}, W = 3.44074 \cdot 10^{-6}, k_e = 3.125$).

Using the realistic film distributions as inputs for the capacitance calculations presented in Sec.3, it is possible to calculate a more realistic capacitance distribution as shown in Figure 9. In the region of the PETRUSEVICH-pressure-spike the local capacitance is usually higher which may be due to the pressure dependent relative permittivity of the lubricant (see Sec. 3.3.1) and the lower film thickness region. There is also a discontinuity at boundaries between the region that is completely filled with lubricant and the region that has a mixture of lubricant and air (see Figure 2) due to the series connection of different permittivities. This can be explained by the series connection of the relative permittivities of lubricant and air. The total capacitance of the contact area $C_{\mathrm{Hertz,h_{real}}}$ is then a summation of all the local parts shown in Figure 9.

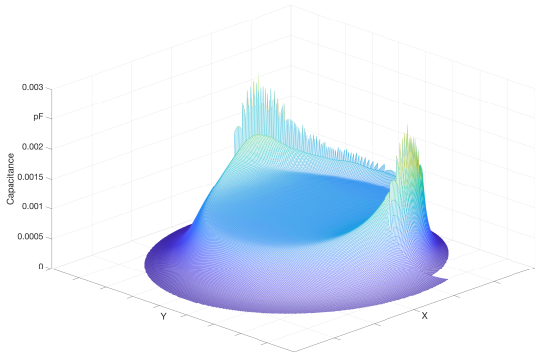

Figure 9: *Capacitance distribution of an EHL contact result of the multigrid-calculation* ($U = 0.562 \cdot 10^{-11}, G = 0.46154 \cdot 10^{4}, W = 3.44074 \cdot 10^{-6}, k_e = 3.125$).

In order to determine the factor k_{vh}, it is necessary to calculate the analytically determinable HERTZ'ian capacitance $C_{\mathrm{Hertz,h_c}}$, which is solely based on the central film thickness as shown in Eq. (3). For the calculation, the same input parameters are used as for the simulation. The pressure distribution is calculated according to the HERTZ'ian approach and the influence of the PETRUSEVICH-pressure-spike is neglected.
With both calculated quantities, the k_{vh} factor can be calculated according to Eq. 8. With the help of all results of the simulation, a system of equations can be set up to optimize the non-linear least squares using e.g. the LEVENBERG-MARQUARDT-algorithm [43, 44] in order to find an equation that matches the simulated results the best.
A total of around 900 simulations were used for the evaluation. The range of values is shown in Table 3. The Formula to be determined is similar to the EHL film thickness formulae by DOWSON and HIGGINSON. The exponents of the dimensionless parameters were determined using the optimization algorithm:

$$k_{vh} = 0.7772 \cdot U^{0.0451} \cdot G^{0.1522} \cdot W_p^{-0.0245} \cdot k_e^{-0.0921} \quad (52)$$

Figure 10 shows the progression of k_{vh} as functions of the dimensionless parameters U, G, W, k_e. It can be seen that the factor in the examined area is in large parts approximately one. Accordingly, if the more realistic film thickness distribution is taken into account, the capacitance of the HERTZ'ian contact area is increased over a wide range compared to the capacitance, in which only h_c is taken into account. In addition, the ratio k_{vh} increases as the ellipticity factor or the load parameter W is reduced, as well as when the material G or the speed parameter U is increased. In the range of low speeds it is possible that the factor drops below one. This is due to the fact that in the simulated film thickness distribution at very low speeds, the mean film thickness

in the HERTZ'ian contact falls below the value of the central film thickness.

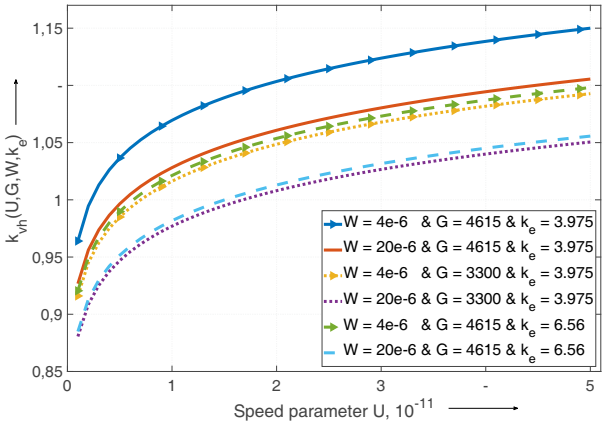

Figure 10: *Function of factor k_{vh} plotted over the speed parameter U with a variation of the load parameter W, material parameter G and the ellipticity k_e.*

4.2. Determination of Factor k_c

Analogously to the determination of the factor k_{vh}, the factor k_c, which describes the ratio of the HERTZ'ian contact capacitance in comparison to the total capacitance of a single contact (see Eq. (4)), was determined. Therefore it is firstly necessary to calculate the capacitance of the HERTZ'ian contact area using only the central film thickness, as described in Sec. 4.1. Secondly it is necessary to add up all incremental parts of the simulation using the realistic film thickness distribution, of the inner and outer regions of the EHL contact.

Similar to factor k_{vh}, factor k_c can be approximated using the following empirical formula based on numerical simulations:

$$k_c = 9.5923 \cdot U^{0.3305} \cdot G^{0.3413} \cdot W_p^{-0.3342} \cdot k_e^{0.1391} \quad (53)$$

The variation of the factor k_c over various range of the dimensionless parameters is displayed in Figure 11. The increase in k_c in terms of speed parameter U agrees with the behaviour described by JABLONKA and GLOVNEA [7]. The higher the film thickness, the greater the influence on the capacitance from the regions outside of the contact. The film thickness increases, for example, at higher speed or lower loads. Due to an increased film thickness the proportion of the region outside the HERTZ'ian contact zone in the total capacitance increases.

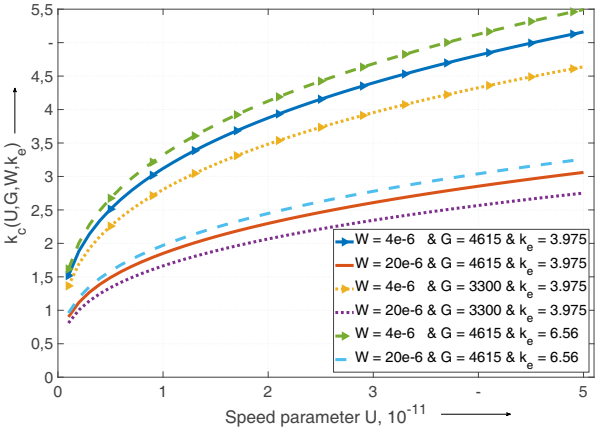

Figure 11: *Function of factor k_c plotted over the speed parameter U with a variation of the load parameter W, material parameter G and the ellipticity k_e.*

5. Application to Rolling Bearings and Discussion

Figures 12 to 14 show the comparison between measured capacitances by one of the authors FURTMANN [6] for a rolling bearing and the analytical results using the developed approaches in this study. Generally, a good agreement under axial load was achieved. The results under radial and combined load show a good qualitative progression but they are smaller than the measured values. This may be due to the selected operating bearing clearance for the calculation, which is discussed in the following.

The bearing capacitance was measured by a method developed by FRANKE and WITTEK [21, 20]. A voltage step is applied between the bearing inner- and outer-ring, which are separated by the EHL films (capacitor like behaviour). By recording and analysing the voltage during the charging process, the total capacitance of the bearing and, in a further step, the average film thickness can be determined. Note that this method only works reliably as long as there are no asperity contacts between the two surfaces; otherwise, the asperity contacts would short-circuit the contact and therefore it would fail to charge the capacitor.

A 75W-90 gear oil was used for the measurements. The Figures 12 to 14 show a typical behaviour of measured capacitances. The physical properties of this oil can be found in Table 1. The further the operating conditions are in the regime of mixed or starved lubrication, the higher the standard deviation due to short-term asperity contacts between the two surfaces. The influence of starvation is also visible in Figures 12 and 13. Due to the relatively high viscosity at a lower temperature of 20 °C, the oil cannot flow back into the raceway as quickly as for example at 40 °C with a lower viscosity (see Figure 14). This starvation behaviour can be reproduced very well by the approaches presented and is in line with the measurements. It should be pointed out that the results were calculated using a theoretical mean operating bearing clearance of +3.5 µm. The operating clearance directly influences the calculable load distribution in the bear-

ing [45, 46]. Under radial load, for example, the load for the individual rolling element can be reduced by a intentionally applied preload of the bearing. This in return directly influences the calculable capacitance, because more rolling elements form a contact zone [47, 48].
Figure 12 shows the results for an axially loaded 6008 DGBB, where every rolling element is loaded equally and it is easier to calculate the bearing capacitance, see for example [9, 6].

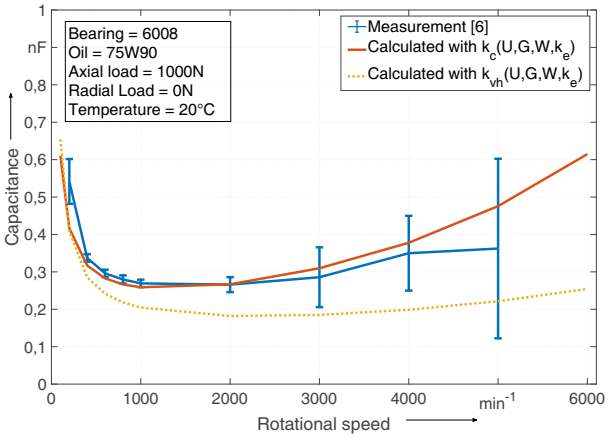

Figure 12: *Comparison between measurement and calculation under axial load with a theoretical mean operating clearance of +3.5 µm.*

Figure 13 shows the comparison between measurements and calculation for a 6008 bearing under a radial load. The calculation of the capacitance under radial load slightly underestimates the capacitances measured in the experiments. However, the overall qualitative progression is in a good approximation.

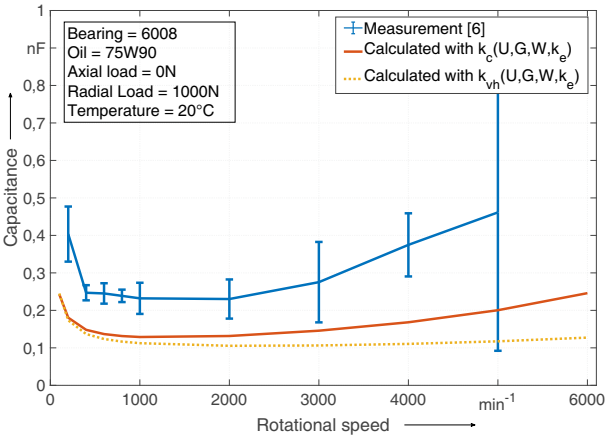

Figure 13: *Comparison between measurement and calculation under radial load with a theoretical mean operating clearance of +3.5 µm.*

For a combined load situation as shown in Figure 14, the results show a similar behaviour as under radial load in Figure 13. Overall the approach that uses the k_c-factor shows a better result compared to the k_{vh}-factor.

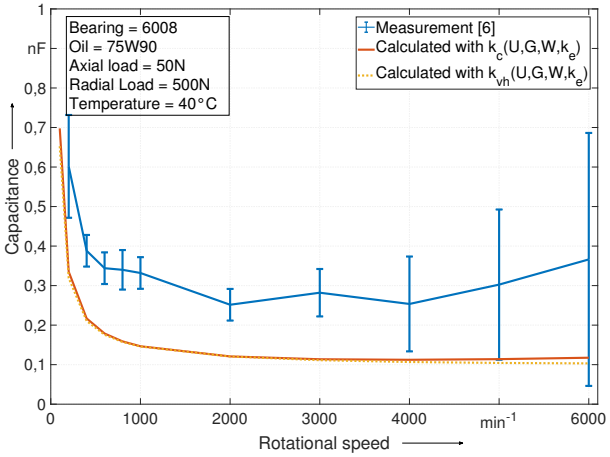

Figure 14: *Comparison between measurement and calculation under combined load with a theoretical mean operating clearance of +3.5 µm.*

The difference between measurements and calculations may be a result of the selected bearing clearance on which the load zone calculation is based. The actual operating bearing clearance of FURTMANN's experiments is unknown, which is the reason why the calculations were conducted for the mean operating clearance of +3.5 µm. As already mentioned, the HERTZ'ian contact areas have a large influence on the total capacitance calculation of a contact. A radial load creates a load zone depending on the size of the internal clearance, so that either more or fewer rolling elements carry the applied load [49]. The larger this load zone, the greater the total capacitance of a bearing as there are more HERTZ'ian contact areas. The influence of the internal clearance (from -9 µm to +16 µm) on the total capacitance of a radially- and axially-loaded bearing is shown in Figure 15 and 16, respectively (see the hatched area). If all tolerances in the system are taken into account, i.e. the fit of the bearing seats, the bearing internal clearance class and the operating temperature, there is a range between the minimum and maximum theoretical operating internal clearance. It becomes clear that the influence of the bearing clearance under radial load has a greater influence on the total capacitance than under axial load.
Under axial load, all rolling elements are loaded equally, which means that only the contact force and angle change when the operating bearing clearance is lowered or raised. While, at a radial loading condition, the amount of loaded rolling elements varies because the size of the load zone increases or decreases.

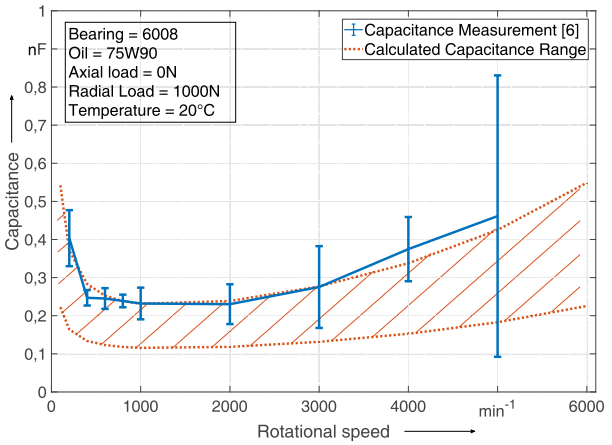

Figure 15: *Effect of internal clearance on the calculated total capacitance of a radially loaded DGBB. The hatched area shows the range between the theoretical minimum operating bearing clearance of -9 µm and the theoretical maximum operating bearing clearance of +16 µm for the given tolerances.*

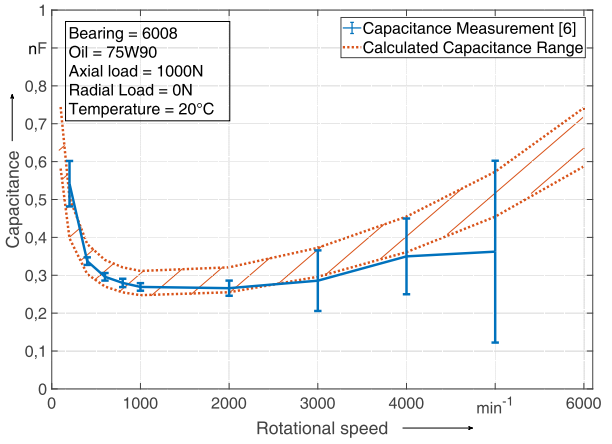

Figure 16: *Effect of internal clearance on the calculated total capacitance of an axially loaded DGBB. The hatched area shows the range between the theoretical minimum operating bearing clearance of -9 µm and the theoretical maximum operating bearing clearance of +16 µm for the given tolerances.*

6. Conclusion and Outlook

In this study, two approaches were presented with which it is possible to calculate the capacitance of a DGBB in order to estimate the electrical bearing load in drive systems. The k_c-factor describes the ratio between the total capacitance of an EHL contact and the capacitance of the HERTZ'ian contact using only the central film thickness. The k_{vh}-factor describes the relationship between the HERTZ'ian contact capacitance using the real film distribution and the HERTZ'ian contact capacitance using exclusively the central film thickness.

The k_{vh}-factor considers the influence of the minimum film thickness on the total capacitance of a HERTZ'ian contact. As can be seen in Figure 10, the factor is always around 1 and therefore has only a very small influence on the capacitance of a contact and an entire rolling bearing. The influence of the minimum lubricant film thickness on the capacitance is therefore negligible. In comparison to the k_c-factor, the k_{vh}-factor additionally requires the calculation of the deformations of the areas outside the HERTZ'ian contact zone. Therefore the k_c-factor is easier to use. In addition, the results using the k_c-factor showed a better agreement with the measured results compared to the k_{vh}-factor. To conclude, it summarizes which formulae are needed in order to calculate the capacitance of an EHL contact and a rolling bearing using either the k_c- or k_{vh}-factor.

Analytical Method using k_c-Factor

Using the k_c-factor (Eq. (53)), the total capacitance of a contact can be calculated using Eq. (5). The needed HERTZ'ian contact area can be calculated with the aid of the HERTZ'ian half-widths a and b (Eqs. (21) and (22)). The film gap between the raceway and the rolling element can be calculated using the EHL-Eq. (15) with additional reduction factors, see Eq. (28), (30) and (34). Finally, the temperature and pressure dependences of the relative permittivity of lubricants has to be determined. Either Eq. (40) or (41) can be used for this.

Analytical Method using k_{vh}-Factor

With the aid of the k_{vh}-factor (Eq. (52)), the height distribution of the whole contact has to be calculated. This includes the HERTZ'ian contact as well as the regions outside the contact ellipse that also experiences a change in geometry. The total capacitance is then calculated using Eq. (10). To calculate the deformation outside the HERTZ'ian zone analytically it is necessary to use an approximation method like the one described in Eq. (39). The central film thickness of the HERTZ'ian contact area is calculated analogous to the k_c-method using Eq. (15) modified with Eq. (28), (30) and (34). Again in analogy to the previously introduced method, the relative permittivity is calculated according to Eq. (40) or (41).

To further improve the model, it would be useful to take a closer look at the temperature distribution in the contact, especially when there is slide-to-roll ratio. As described in Sec. 3.3.1, the permittivity of the lubricant is strongly dependent on density and therefore on temperature. Due to local shear stress in the contact and the Heathcote- or drill-slip, temperature rise as shown in [50, 51, 52] occur. The presented model assumes an isothermal contact, whereby the permittivity only changes locally due to the pressure distribution. Therefore, it is likely that by taking into account the temperature distribution effected by the local shear stress, the calculation results could be further improved.

Acknowledgements

This work was executed at the Leibniz University Hannover, Germany. The authors would like to thank the "Otto von Guericke"-Research Association (AiF) for their financial support of the project (Grant No. 20496 N). The authors also would like to thank the Flender GmbH for permission to publish this paper.

References

[1] M. Habibullah, D. D.-C. Lu, D. Xiao, M. F. Rahman, Finite-State Predictive Torque Control of Induction Motor Supplied From a Three-Level NPC Voltage Source Inverter, IEEE Transactions on Power Electronics 32 (1) (2017) 479–489. doi:10.1109/TPEL.2016.2522977.

[2] V. Hausberg, Elektrische Lagerbeanspruchung umrichtergespeister Induktionsmaschinen, no. 324 in Fortschritt-Berichte VDI Reihe 21, Elektrotechnik, VDI, Düsseldorf, 2002.

[3] A. Mütze, Bearing Currents in Inverter-Fed AC-Motors, Ph.D. thesis, Technische Universität Darmstadt (2004).

[4] B. J. Hamrock, D. Dowson, Ball Bearing Lubrication: The Elastohydrodynamics of Elliptical Contacts, Wiley, New York, 1981.

[5] N. Bader, H. Liu, B. B. Zhang, G. Poll, Film Thickness Measurements in EHL-Contacts using Capacitance Measurements, in: 46th Leeds-Lyon Symposium on Tribology 2019, Lyon, France., 2019.

[6] A. Furtmann, Elektrische Belastung von Maschinenelementen im Antriebsstrang, Ph.D. thesis, Leibniz Universität Hannover (2017).

[7] K. Jablonka, R. Glovnea, J. Bongaerts, Evaluation of EHD films by electrical capacitance, Journal of Physics D: Applied Physics 45 (38) (2012) 385301. doi:10.1088/0022-3727/45/38/385301.

[8] R. Gohar, Elastohydrodynamics, 2nd Edition, Imperial College Press, London, 2001.

[9] N. Bader, A. Furtmann, H. Tischmacher, G. Poll, Capacitances and lubricant film thicknesses of grease and oil lubricated bearings, in: STLE Annual Meeting & Exhibition, At Atlanta, Georgia (US), Vol. 72, 2017.

[10] E. Wittek, M. Kriese, H. Tischmacher, S. Gattermann, B. Ponick, G. Poll, Capacitances and lubricant film thicknesses of motor bearings under different operating conditions, in: I. Staff (Ed.), 2010 XIX International Conference on Electrical Machines, I E E E, 2010, pp. 1–6. doi:10.1109/ICELMACH.2010.5608142.

[11] T. Maruyama, K. Nakano, In Situ Quantification of Oil Film Formation and Breakdown in EHD Contacts, Tribology Transactions 61 (6) (2018) 1057–1066. doi:10.1080/10402004.2018.1468519.

[12] T. Maruyama, M. Maeda, K. Nakano, Lubrication Condition Monitoring of Practical Ball Bearings by Electrical Impedance Method, Tribology Online 14 (5) (2019) 327–338. doi:10.2474/trol.14.327.

[13] M. Barz, Die Schmierfilmbildung in fettgeschmierten schnellaufenden Spindellagern, Ph.D. thesis, Leibniz Universität Hannover, Hannover (1996).

[14] A. Cameron, R. Gohar, O. A. Saunders, Theoretical and experimental studies of the oil film in lubricated point contact, Proceedings of the Royal Society of London. Series A. Mathematical and Physical Sciences 291 (1427) (1966) 520–536. doi:10.1098/rspa.1966.0112.

[15] H. Cen, P. M. Lugt, Film thickness in a grease lubricated ball bearing, Tribology international 134 (2019) 26–35. doi:10.1016/j.triboint.2019.01.032.

[16] R. Glovnea, M. Furtuna, Y. Nagata, J. Sugimura, Electrical Methods for the Evaluation of Lubrication in Elastohydrodynamic Contacts, Tribology Online 7 (1) (2012) 46–53. doi:10.2474/trol.7.46.

[17] R. S. Heemskerk, K. N. Vermeiren, H. Dolfsma, Measurement of Lubrication Condition in Rolling Element Bearings, A S L E Transactions 25 (4) (1982) 519–527. doi:10.1080/05698198208983121.

[18] K. Jablonka, R. Glovnea, J. Bongaerts, Quantitative measurements of film thickness in a radially loaded deep-groove ball bearing, Tribology International 119 (2018) 239–249. doi:10.1016/j.triboint.2017.11.001.

[19] P. Brüser, Untersuchungen über die elastohydrodynamische Schmierfilmdicke bei elliptischen Hertzschen Kontaktflächen, Ph.D. thesis, Technische Universität Carolo-Wilhelmina zu Braunschweig, Braunschweig (1972).

[20] E. Wittek, Charakterisierung des Schmierungszustandes im Rillenkugellager mit dem kapazitiven Messverfahren, Ph.D. thesis, Leibniz Universität Hannover, Hannover (2016).

[21] J. E. Franke, Der Einfluß der Schmierfettzusammensetzung auf das tribologische Verhalten schnellaufender Wälzlager, Ph.D. thesis, Universität Hannover (1999).

[22] T. Harris, M. Kotzalas, Essential Concepts of Bearing Technology, CRC Press, [Place of publication not identified], 2019.

[23] Baldor, Inverter-Driven Induction Motors Shaft and Bearing Current Solutions Industry White Paper, Fort Smith (USA) (2007).

[24] H. Tischmacher, O. Kartashov, Simulation von Lichtbogenentladungen in Wälzlagern von Elektromotoren Zur Interpretation von Experimentellen Ergebnissen an Einem Lagerversuchsstand, 32nd Edition, 2014.

[25] L. E. Murch, W. R. D. Wilson, A Thermal Elastohydrodynamic Inlet Zone Analysis, Journal of Lubrication Technology 97 (2) (1975) 212–216. doi:10.1115/1.3452559.

[26] SKF, The SKF Model for Calculating the Frictional Moment, 2018.

[27] O. Kreil, Einfluss der Oberflächenstruktur auf Druckverteilung und Schmierfilmdicke im EHD-Kontakt, Ph.D. thesis, Technische Universität München (2013).

[28] S. P. Timošenko, J. N. Goodier, Theory of Elasticity, 3rd Edition, Engineering Societies Monographs, McGraw-Hill, New York, 1987.

[29] J. F. Skinner, E. L. Cussler, R. M. Fuoss, Pressure dependence of dielectric constant and density of liquids, The Journal of Physical Chemistry 72 (3) (1968) 1057–1064. doi:10.1021/j100849a048.

[30] J. D. Jackson, Classical Electrodynamics, 3rd Edition, Wiley, New York, 1999.

[31] A. A. Bondi, Physical Chemistry of Lubricating Oils., Book Division, Reinhold Pub. Corp., New York, 1951.

[32] R. Schrader, Die Schmierfilmbildung von additivierten Mineralölen, synthetischen Schmierfilmflüssigkeiten und Schmierfetten im elastohydrodynamischen Wälzkontakt, Ph.D. thesis, Leibniz Universität Hannover (1988).

[33] B. Bode, Entwicklung eines Quarzviskosimeters fuer Messungen bei hohen Druecken, Ph.D. thesis, Technische Universität Clausthal (1984).

[34] B. Bode, Modell zur Beschreibung des Fliessverhaltens von Flüssigkeiten unter hohem Druck, Tribologie und Schmierungstechnik 35 (5) (1989) 256–261.

[35] D. Dowson, G. R. Higginson, Elasto-Hydrodynamic Lubrication: The Fundamentals of Roller and Gear Lubrication, Pergamon Press, 1966.

[36] P. G. Tait, Scientific Papers, University Press, Cambridge, 1898.

[37] A. T. J. Hayward, Compressibility equations for liquids: A comparative study, British Journal of Applied Physics 18 (7) (1967) 965–977. doi:10.1088/0508-3443/18/7/312.

[38] S. Bair, C. McCabe, High Pressure Rheology for Quantitative Elastohydrodynamics - 1st Edition, 1st Edition, no. 54 in Tribology and Interface Engineering Series, Elsevier, Amsterdam ; Boston, 2007.

[39] A. Lubrecht, Numerical solution of the EHL line and point contact problem using multigrid techniques, Ph.D. thesis, University of Twente. Enschede, The Netherlands (1987).

[40] C. H. Venner, Multilevel solution of the EHL line and point contact problems, Ph.D. thesis, University of Twente. Enschede, The Netherlands (op.1991).

[41] H. C. Liu, B. B. Zhang, N. Bader, F. Guo, G. Poll, P. Yang, Crucial role of solid body temperature on elastohydrodynamic film thickness and traction, Tribology International 131 (2019) 386–397. doi:10.1016/j.triboint.2018.11.006.

[42] A. Petrusevich, Principal conclusions from contact-hydrodynamic theory of lubrication Izv. Akad. Nauk SSSR. Otd. Tekh. Nauk (1951) 209–233.

[43] K. Levenberg, A method for the solution of certain non-linear problems in least squares, Quarterly of Applied Mathematics 2 (2) (1944)

164–168. doi:10.1090/qam/10666.

[44] W. Marquardt, E. Dupont, R. Bennett, G. Burrell, An algorithm for least-squares estimation of nonlinear parameters, Jornal of Society for Industrial and Applied Mathematics Vol. 2 (2) (1963) 431–441. doi:10.1137/0111030.

[45] S. Andréason, Theoretische Grundlagen für die Berechnung von mit Kräften und Momenten belasteten Rillenkugellagern, Konstruktion 21 (3) (1969).

[46] J. M. de Mul, J. M. Vree, D. A. Maas, Equilibrium and Associated Load Distribution in Ball and Roller Bearings Loaded in Five Degrees of Freedom While Neglecting Friction—Part I: General Theory and Application to Ball Bearings, Journal of Tribology 111 (1) (1989) 142–148. doi:10.1115/1.3261864.

[47] E. Wiche, Radiale Federung von Wälzlagern bei beliebiger Lagerluft, Konstruktion (5) (1967) 184–192.

[48] R. Böttcher, Untersuchungen zum Betriebsverhalten radial vorgespannter Zylinderrollenlager, Ph.D. thesis, Leibniz Universität Hannover (2018).

[49] F. B. Oswald, E. V. Zaretsky, J. V. Poplawski, Effect of Internal Clearance on Load Distribution and Life of Radially Loaded Ball and Roller Bearings, Tribology Transactions 55 (2) (2012) 245–265. doi:10.1080/10402004.2011.639050.

[50] H. S. Nagaraj, D. M. Sanborn, W. O. Winer, Surface Temperature Measurements in Rolling and Sliding EHD Contacts, A S L E Transactions 22 (3) (1979) 277–285. doi:10.1080/05698197908982925.

[51] K. H. Kim, F. Sadeghi, Three-Dimensional Temperature Distribution in EHD Lubrication: Part I—Circular Contact, Journal of Tribology 114 (1) (1992) 32–41. doi:10.1115/1.2920864.

[52] R. S. A. Grieve, H. A. Spikes, Temperature and Shear Stress in Thin Film EHD Contacts, in: D. Dowson, M. Priest, C. M. Taylor, P. Ehret, T. H. C. Childs, G. Dalmaz, A. A. Lubrecht, Y. Berthier, L. Flamand, J. M. Georges (Eds.), Tribology Series, Vol. 38 of Thinning Films and Tribological Interfaces, Elsevier, 2000, pp. 511–522. doi:10.1016/S0167-8922(00)80155-8.